Multimedia Tools and Applications (2024) 83:3567–3584
https://doi.org/10.1007/s11042-023-15688-0

Lung cancer segmentation from CT scan images using modified mayfly optimization and particle swarm optimization algorithm

S. Poonkodi[1] **· M. Kanchana**[2]

Received: 7 February 2022 / Revised: 25 May 2022 / Accepted: 23 April 2023 /
Published online: 18 May 2023

Abstract
The development of a computer-aided detection system is a critical component of clinical decision-making As the death rate grows, cancer has become a major concern for both men and women. The radiologists need to accurately pinpoint the region of the lung tumor to offer proper radiation therapy for lung cancer patients. Due to low-image quality, higher computational difficulties, and other reasons, the existing lung cancer segmentation methods failed to provide better segmentation accuracy. To overcome these challenges, we proposed a novel approach for lung tumor segmentation. Initially, the input CT scan image contrast level is increased using histogram equalization (HE) during pre-processing. The adaptive bilateral filter (ABF) provides enhanced CT scan images for de-noising. Next to pre-processing, we introduced an ensemble deep convolutional neural network (EDNN) based on Modified mayfly optimization and modified particle swarm optimization (M^2PSO) algorithm for the segmentation of lung cancer from the pre-processed CT images. The proposed model accurately segments the lung disease tumor without manual supervision and the need for fully annotated data. Finally, the measures like dice similarity score (DSS), precision, sensitivity, dice loss, and generalized dice loss analyze the performance of the proposed model. Based on the experimental investigations, the proposed EDCNN- M^2PSO algorithm demonstrated superior performance in terms of lung tumor segmentation than other existing techniques. The proposed model has average accuracy, sensitivity, and precision scores of 97%, 98%, and 98%, respectively. The proposed model's DSS value is 98.6%, which is relatively higher than the existing approaches.

Keywords Lung cancer · Automatic segmentation · Lung computed tomography · Ensemble Deep Convolutional Neural Network · Modified mayfly optimization

✉ S. Poonkodi
rkpoonkodi@gmail.com

[1] Department of Computing Technologies, School of Computing, SRM Institute of Science and Technology, Kattankulathur, India

[2] Department of Computing Technologies, School of Computing, SRM Institute of Science and Technology, Kattankulathur, India

1 Introduction

Because false mutations radically alter human existence, the genetic issue affects the majority of people in new technological breakthroughs. The DNA functions and structure are totally changed based on the false mutation [15]. External variables such as chemical gas exposure, alcohol consumption, and population air-breathing all contribute to abnormal mutation. Mainly, tumors are created based on the mutation of the abnormal cell (DNA) that arises in different places of the human body like the brain, breast, skin, and lung [6]. Due to the external factors, the most caused disease is lung cancer (LC) among the several tumors that generally affects there spiratory system of human.

In the world, the most popular kinds of malignant tumor are lung cancer, which takes second place based on a study of the United States. The two kinds of LC are non-small cell lung cancer (NSCLC) and small cell lung cancer (SCLC) respectively [27]. Lung cancer diagnoses are performed via various processes like CT, X-ray, isotope, and MRI. Two recognizable anatomic imaging are Computer Tomography (CT) and X-ray chest radiography [17]. The presence of disease is recognized and identified by radiologists and physicians using CT images thereby describing the severity of diseases. The scan time is shortened in which the spiral scans introduce a volumetric CT technique.

With the advancement of CT technology, high-resolution CT examinations have become the imaging modality of choice for the diagnosis and recognition of lung diseases [2]. Improved anatomic resolution with lung imaging based on High-Resolution Computed Tomography (HRCT) [18]. Several computer-aided diagnostic models and detection techniques for lung cancer segmentation have been developed during the last several decades [11]. The existing techniques like deep learning (DL), recurrent 3d-denseness (R3-D), hybrid segmentation network (HSN), deep active learning (DAL), etc. are used for lung cancer segmentation [16]. The development of computer-aided systems promotes the necessity for objective and reliable analysis. Fast and accurate lung cancer segmentation is the major aim of this study.

The early-stage lung cancer patient often possesses no symptoms which increases the complexity of disease diagnosis. Hence early diagnosis plays a main role in lung cancer diagnosis. The CT scans are mainly utilized in this work to overcome the shortcomings (low contrast, similar tissue absorption, and plane overlap) associated with the two-dimensional X-rays since it provides high-density resolution. The lung disease can be identified in an early stage via the CT images since it helps to identify the normal and malignant lung nodules accurately in a non-invasive manner. Because CT scan images contain large scanning layers, the radiologist encounters numerous obstacles while analyzing them. Processing mass CT images is often time-consuming, involves extensive manual intervention, and results in incorrect results. Hence the clinical needs cannot be met by manual segmentation and it needs an artificial intelligence technique which can identify the tumor lesions in a massive dataset [10].

As a result, manual segmentation cannot meet the clinical needs, and an artificial intelligence technique that can identify tumor lesions in a large dataset is required. The Convolutional Neural Network (CNN) architecture has demonstrated its ability to overcome these challenges by dynamically monitoring the liver tumor areas, resulting in accurate diagnosis. Despite the fact that the CNN architecture has many advantages, it has a number of drawbacks, including low generalization and interpretation capabilities, low robustness, and data accessibility constraints. This paper presents a modified

optimization algorithm to overcome the complexities associated with the CNN architecture. The major contribution of this study is summarized below:

- During pre-processing, the histogram equalization (HE) and adaptive bilateral filter (ABF) are used to increase the CT scan image contrast level and enhance CT scan images for de-noising.
- We combined and used Modified mayfly optimization and modified particle swarm optimization (M^2PSO) algorithms thereby obtaining the improved segmentation accuracy.
- The performance of ensemble deep convolutional neural network (EDNN) for lung cancer segmentation is enhanced by combining M^2PSO algorithms.
- The Shandong Cancer Hospital Affiliated to Shandong University (SHFSU) offers dataset image information as well as measurements such as dice similarity score (DSS), accuracy, sensitivity, dice loss, and generalized dice loss to assess the efficacy of the proposed model.

The rest of the article is shortened as follows: The literature survey is analyzed in Sect. 2. Section 3 describes the proposed methodology. The experimental investigations are examined in Sect. 4 and Sect. 5 concludes the article.

This study proffers solutions to the issues of high computational cost due to the implementation of facial expression recognition by providing a model close to the accuracy of the state-of-the-art model. The study concludes that deep learning-enabled facial expression recognition techniques enhance accuracy, better facial recognition, and interpretation of facial expressions and features that promote efficiency and prediction in the health sector.

2 Related works

Deep learning (DL) methods were suggested by Li et al. [16] for the segmentation of lung cancer. From 200 patients, an annotated dataset of 50 test images and 150 training images were used to focus the cancer tissue segmentation. The metrics like DICE coefficient, specificity, sensitivity, accuracy, and precision were evaluating the performance of DL techniques thereby obtaining better segmentation accuracy with higher computational complexities. Men et al. [20] introduced deep active learning (DAL) for lung cancer segmentation. Depending upon the deep learning activity, the candidate set provides the selected quality images. The Hausdorff distance and Dice are the segmentation metrics to validate the performance of the DAL model. Various sensitivity, balanced, and accuracy outputs were obtained with respect to the right lung, left lung, spinal cord, esophagus, and heart. But, this method had taken a larger execution time for implementation.

The recurrent 3d-denseunet (R3-D) was introduced by Kamal et al. [14] for the segmentation of the lung cancer tumor region. The fine-grained Spatio-temporal information was extracted with the help of multiple Convolutional Long Short-Term Memory (CLSTM). Several 3D-convolutional layers have a decoder and encoder blocks. In practice for this task, various loss functions based extensive ablation study was performed. The segmentation result with a 0.7228% average dice score was achieved than other state-of-art techniques but the segmentation accuracy is lower. A hybrid segmentation network (HSN) was introduced by Chen et al. [9] for small cell lung cancer segmentation. The severe class data imbalance problem was tackled by utilizing the generalized Dice loss function (GDLF). Depending upon the experimental results, the HSN model

provided 0.909% precision, 0.872% sensitivity score, and 0.888% dice score values. This method failed to include the healthy people scan in the dataset.

Skourt et al. [26] suggested deep neural networks (DNN) for lung segmentation CT images. The symmetric expanding path was recovered and high-level information was extracted via the contracting path. The dice-coefficient index was 0.9502 and proved accurate segmentation based on the U-net architecture. The computational complexity and time delay were higher. For chest X-ray analysis of lung cancer, Gordienko et al. [12] suggested the deep learning (DL) model. Without rib and clavicle shadows, the original JSRT dataset was used to perform both training and validation. In the simplified configuration, the pre-processing techniques were considered to demonstrate usefulness and high-efficiency results. This method is unsuitable to train larger and more complicated image models.

The K-nearest neighbor (KNN) [23], deep learning (DL) [24], and Convolutional Neural networks (CNN) [8] tend to be promising in cancer tumor segmentation. However, the features learned by these models are often redundant. Even though, these works offer improved performance still they need modifications to improve the accuracy of the lung cancer segmentation and search the smaller homogeneous regions. The summary of the literary works is presented in Table 1.

3 Proposed methodology

This section proposed a novel approach for lung tumor segmentation. Initially, the input dataset image is fed for pre-processing. From the pre-processed image, the lung tumors are segmented through a deep convolutional neural network with a modified mayfly-based modified particle swarm optimization (M^2PSO) algorithm. The overall proposed architecture is depicted in Fig. 1.

3.1 Pre-processing

Histogram equalization (HE) enhances the input CT scan image contrast during pre-processing. Equation (1) shows the contrast enhancement of the CT image (AI) by applying histogram equalization.

$$AI = {}^{\Delta P}/_{L} \tag{1}$$

where, IN and TP are the available intensity m with a number of pixels and the total number of pixels. The ranges from 0 to 256 are the pixel intensities. For available intensity, the normalized histogram image bin (I) is denoted as M. Image is divided into multiple sub-regions and recovering the image contrast. Transform the specified target histogram with the intensity of all sub-regions independently to fulfill [19].

For de-noising, enhanced CT scan images are obtained by applying an adaptive bilateral filter (ABF). Equation (2) shifts the range filter on the histogram by adding a counterbalance to the range [31].

$$ABF_{y_0,z_0} = \sum_{y=y_{0-M}}^{y_0+M} \sum_{z=z_0}^{z_0+M} \exp\left(-\frac{(y-y_0)^2+(z-z_0)^2}{2\nabla_c^2}\right) + exp\left(-\frac{(H[y_0z_0]-H[y_0z_0-\chi[y_0z_0]^2])}{2\nabla_e^2[y_0z_0]}\right) \tag{2}$$

Table 1 Summarization of the literary works

Reference	Technique used	Advantage	Limitation
[16]	DL	Better segmentation accuracy	Higher computational complexity
[20]	DAL	Automatically detects contour errors	Large execution time
[14]	R3-D, CLSTM	End-to-end training of CNN	Failed to implement dimensionality reduction
[9]	HSN, GDLF	Addresses the class imbalance problem	Absence of healthy samples in the dataset
[26]	DNN, U-net	Accurate segmentation outcomes	Increased delay and computational complexity
[12]	DL model	The model offers better accuracy and losses	Ineffective for training large and complex image models
[24]	ConvNet	Improved accuracy and efficiency in the health care	The manual parameter adjustment often minimizes the prediction accuracy
[23]	KNN	Offers improved performance in a large dataset	The error rate cannot be efficiently determined using the K-value
[8]	Structured model pruning and VGG16	Improved memory usage and speed for small datasets without compromising the accuracy	The structured model pruning parameters are not strictly linear with each other

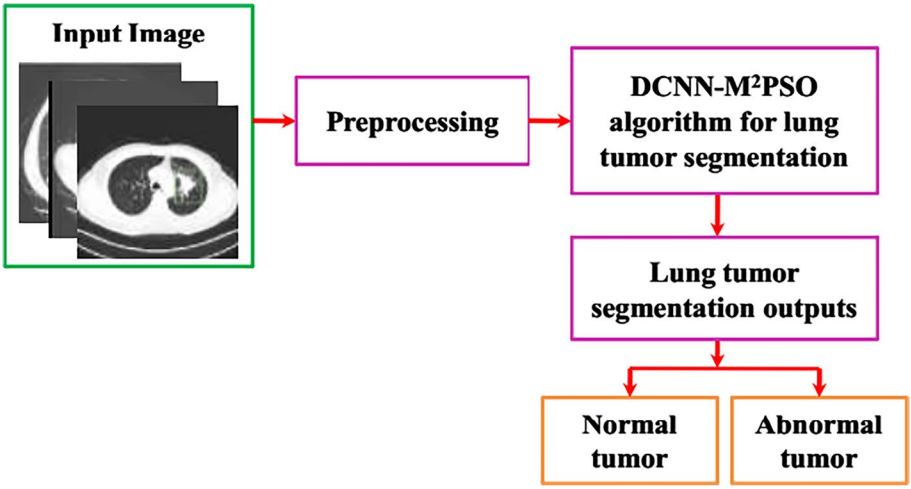

Fig. 1 Overall proposed architecture

From Eq. (2), the index column of a current image pixel and the neighboring pixel row index are defined as z_0 and y. The neighboring pixel column index and the neighboring pixel column index are z and y. The size of the neighboring window is $\xi_{y_0 z_0}$ and the neighboring window pixel is M.

During the process of image acquisition, the CT images are surrounded bya few of the noises that lead to failure nodules detection. Detected abnormalities were incorrectly assumed to be cancer nodules for a while, and additional abnormalities need to be removed for a better and more accurate cancer diagnosis. With the ABF sharpening the CT scan images without causing overrun, the edge slope rises [7]. While improving textures and edges in the images, ABF is able to smooth the noise. When compared to other median and mean filters, the ABF produced good results. The ABF overcome the causes of halo artifacts and objectionable ringing based on issues in conventional filters like under and overshoots around the renders clean. The entire appearance is enhanced and the slope edge in the image is enhanced.

3.2 Lung cancer segmentation

In this study, the lung cancer segmentation is performed using a Deep CNN models-based ensemble approach with Modified Mayfly and modified particle swarm optimization algorithm. The steps involved for lung cancer segmentation is delineated as follows:

3.2.1 Ensemble deep convolutional neural network (EDCNN):

One of the widely used deep learning models is the convolutional neural network (CNN). In an input image, CNN studies various biases and weights relating to different items, allowing it to distinguish between them. The algorithm uses the number of channels, width, and height of an input image in the appearance of a pixel value matrix [29]. A network is made up of layers, and the first layer is a convolutional neural network, which feeds the input image. The convolutional kernel set may be found in the

convolutional layer that covers the small image areas. Equation (3) expresses the convolution operation.

$$Y_c^d = (Z_{z,x} * A_c^d) \tag{3}$$

From this equation, the spatial locality and the input image is expressed as z, x and $Z_{z,x}$. At d^{th}layer, the c^{th} convolutional kernel is A_c^d. The activation and pooling layer along with the convolutional neural network present in a CNN. For analyzing nonlinear image properties, the decision function or activation function has a major role in the activation layer [1]. The image downsampling is performed via pooling layers. Equation (4) expresses the pooling operation.

$$G_c = R_O(Y_{z,x}^c) \tag{4}$$

Based on Eq. (4), the pooling operation type is $R_0(\cdot)$. The c^{th} input and output feature maps are $Y_{z,x}^c$ and G_c. At the end of a network, attach a fully connected layer in which the M number of output classes related to the M-dimensional vector is produced.

A. *AlexNet and VGG-FaceNet:*

The number of CNN parameter optimization models builds up the AlexNet model, which is the deeper of CNN. Extend the feature extraction from 5 (inLeNet) to 7 (in AlexNet) to make the application of CNN to diverse image classifications. While increasing model depth, the issues like vanishing gradient descents and overfitting arise. In the initial layers, introduce large-sized filters and minimize overfitting.

One of the effective design principles of CNN is VGG-FaceNet. Over the input matrix, place the small-sized filters and the larger-sized filters are induced. For image classification and localization, VGG-FcaeNet possesses homogeneous and feature topology. Due to the approximate 140 million parameter applications, it cause by the limitation of higher computational cost.

B. *FlowImageNet and ResNet:*

There are 3 fully connected layers and 5 convolutional layers present in this model. The vanishing descent and overfitting issues are resolved via ReLU activation function. The computational complexities of CNN, AlexaNet, VGG-FaceNet, and FlowImageNet are overcome by using ResNet.

III. *Ensemble*

The patterns in data are highly recognized via neural networks. These networks are sensitive to a particular training data is the drawback. Each time they are trained, the various weight sets are obtained. GASEN, simple averaging, and weighted voting are a few of the ensemble methods. The simple prediction models are surpassed via these techniques. The structure of EDCNN is depicted in Fig. 2.

3.2.2 Modified Mayfly based particle swarm optimization (M^2PSO):

This section describes the modified mayfly-based particle swarm optimization (M^2PSO) algorithm.

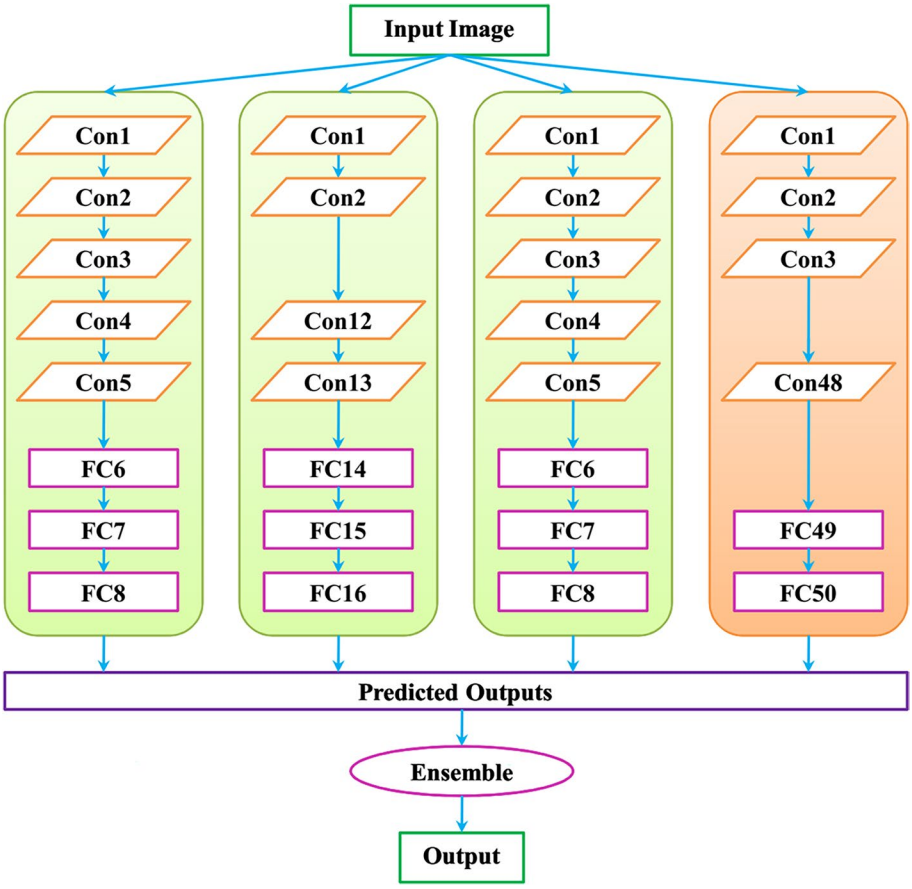

Fig. 2 Structure of EDCNN [29]

A. *Modified Particle Swarm Optimization (MPSO) algorithm:*

While modifying the personal best update, the modified PSO is the enhanced version of the particle swarm optimization (PSO) algorithm. The following section delineates the MPSO algorithm.

(i) The number of decision variables (DV) defines the algorithm parameters. The population size (P_{max}) with the upper and lower bounds are U_p and L_o. The velocity is VE with the weight coefficient are wc_1 and wc_2.

(ii) The initial value with the matrix is similar to the $DV * P_{\max}$. The below equation expresses the vectors based on initial populations [21].

$$Y_{j,k} = L_o + (U_p - L_o) * random\ [0, 1] \tag{5}$$

$$Pa = \begin{bmatrix} Y_{1,1}\ Y_{1,2} & \cdots & Y_{1,DV} \\ Y_{2,1}\ Y_{2,2} & \cdots & Y_{2,DV} \\ \vdots\ \vdots & \ddots & \vdots \\ Y_{P_{\max},1}\ Y_{P_{\max},2} & \cdots & Y_{P_{\max},DV} \end{bmatrix} \tag{6}$$

(iii) The following steps generate the new particle. Equation (7) updates the particle velocity.

$$VE_{j,k}^{t+1} = \beta VE_{j,k}^{t} + D_1 random[0,\ 1] \times \left(Best_{pa_{j,k}}^{\ t} - Y_{j,k}^{t} \right) + D_2 random\ [0,\ 1] \times (Best_{G_{j,k}}^{\ t} - Y_{j,k}^{t}) \tag{7}$$

(iv) Eq. (8) updates the positions of the particles.

$$Y_{j,k}^{t+1} = VE_{j,k}^{t+1} + Y_{j,k}^{t} \tag{8}$$

(v) According to the objective functions, evaluate the new improved vectors. Accept $Y_{j,DV}^{t+1}$ if the fitness of $Y_{j,DV}^{t+1}$ is smaller to $Best_{pa_{j,DV}}^{\ t+1}$ fitness. For next-generation, the new particle replaces if the new particle is unaccepted in the particle best ($Best_{pa_{j,DV}}^{\ t+1}$) updating step.

B *Modified mayfly Optimization (MMO) algorithm:*

Based on the explanations, the Modified Mayfly Optimization (MMO)method is a fresh and new metaheuristic for solving many problems the conventional MMO method has a few issues in obtaining the optimal resolution in some circumstances. A new modification mechanism is provided to overcome this problem in this part. The global best and individual best position is $Best_{Gj}$ and $Best_{po_j}$ if the current candidate position $Y_{j,k}^{t}$ is overlapped. Each candidate stops flying if the preceding candidate velocities are adjacent to zero [25].

In the whale optimization algorithm, derive the updating position from the bubble net searching schemes. Based on the surrounding and moving spiral around the prey, the whale huts its prey based on the whale optimization algorithm. From the preceding time step, j^{th} particle in the d^{th} dimension updates its positions based on the spiral updating policy. Update the candidate position by considering Y_j as the candidate's current positions.

$$Y_j(t+1) = Ce^{al}\cos(2\pi l) + Y_{jk}(t) \tag{9}$$

$$C = |Y_{jk}(t) - Y_{ki}(t)| \tag{10}$$

The spiral shape defines the constant value a. For the j^{th} individual to the best solution, the random values among 0 and 1. For the j^{th} individual to the best solution, the distance is denoted as C. Where, A is the probability factor in the interval 0 and 1.

III. *Modified mayfly based particle swarm optimization (M^2PSO):*

The following steps express the modified mayfly-based particle swarm optimization (M^2PSO) algorithm.

(i) Initialization of MPSO and MMF
(ii) Constraints determine the best solution
(iii) Fitness function evaluation

(iv) The two stages of the MPSO and MMF algorithm select the best solution.
(v) MPSO algorithm selects the $Best_G$

Initialize the population of the MPSO algorithm. Update the particle velocity and position and generate the new particle [4]**.** Calculate new improved vectors depending upon the objective function. The process is repeated till the end of the termination condition is satisfied.

(vi) At the same time, MMF algorithm selects the $Best_G$

Initialize the population of MMF and update the position with spiral movement. Again, update the candidate positions. The procedure is continued at the end of obtaining $Best_G$ solution.

(vii) The ideal solution is classified based on the priority of $Best_G$
(viii) Obtain the optimal best solution

3.2.3 Lung tumor segmentation using (EDCNN-M^{2}PSO)

In general, the accuracy of the EDCNN model's results improves. By combining the distinct outputs of each model, simple averaging yields a single outcome. The average of the results of each model is calculated [13]. But this output has a few limitations with the inaccurate result due to computational complexity, poor segmentation efficiency and etc. Hence, we suggested the M^{2}PSO algorithm to provide better segmentation results because this method has better exploration and exploitation ability with optimal best solution selection and so on [5]. Therefore, the combination of EDCNN- M^{2}PSO algorithm is applied for lung tumor segmentation. The lung tumor segmentation using the proposed EDCNN-M^{2}PSO algorithm is depicted in Fig. 3. From the pre-processed CT scan image, the proposed EDCNN-M^{2}PSO algorithm segments the cancer nodules. The proposed algorithm segments both normal and abnormal lung tumors that mean mild and severe kinds of tumors. In order to diagnosis the disease, distinct areas are analyzed and cancer affected region is segmented from the CT images using the EDCNN-M^{2}PSO algorithm.

4 Result and discussion

This section investigates the performance of the proposed EDCNN with the M^{2}PSO algorithm for lung tumor segmentation. For 50 epochs, train the EDCNN-M^{2}PSO model on 11 GB of RAM with NVIDIA 1080Ti GPU. The working platform of MATLAB software implements the proposed model [5]. Various performance measures and comparative analyses are taken to validate the performance of the proposed method. Table 2 delineates the parameter settings of the proposed model.

4.1 Dataset details

Under the approval of the institutional review board, Shandong Cancer Hospital Affiliated with Shandong University (SHFSU) provides the dataset image details which consists of 134 contrast-enhanced CT images. Based on pulmonary CT investigation, this study uses all CT images by utilizing a Brilliance 128*i* CT scanner by means of a 5-*mm*

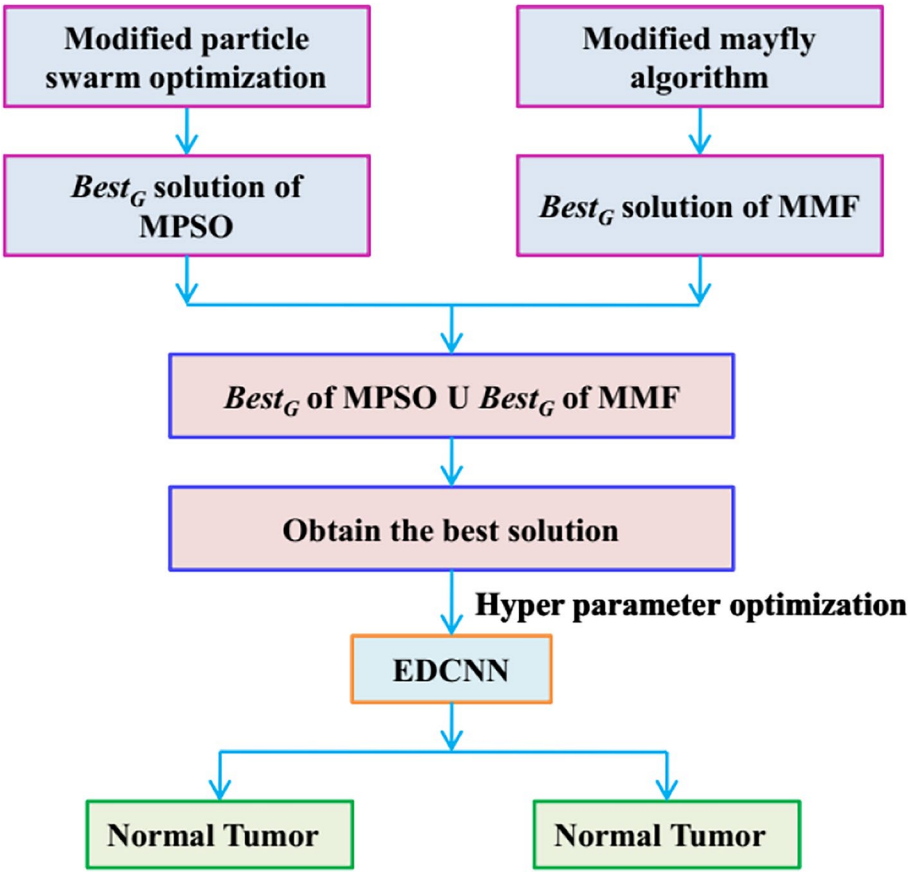

Fig. 3 Proposed EDCNN-M2PSO algorithm for lung tumor segmentation

Table 2 Parameter settings

Models	Parameters	Ranges
ResNet	Number of convolutional layers	48
	Number of fully connected layers	2
	Number of parameters	23,564,712
FlowImageNet	Number of convolutional layers	5
	Number of fully connected layers	3
	Number of parameters	80,283,396
VGG-FaceNet	Number of convolutional layers	13
	Number of fully connected layers	3
	Number of parameters	138,357,544
AlexNet	Number of convolutional layers	5
	Number of fully connected layers	3
	Number of parameters	58,299,140
M^2PSO	Number of population	10
	Maximum number of iterations	50

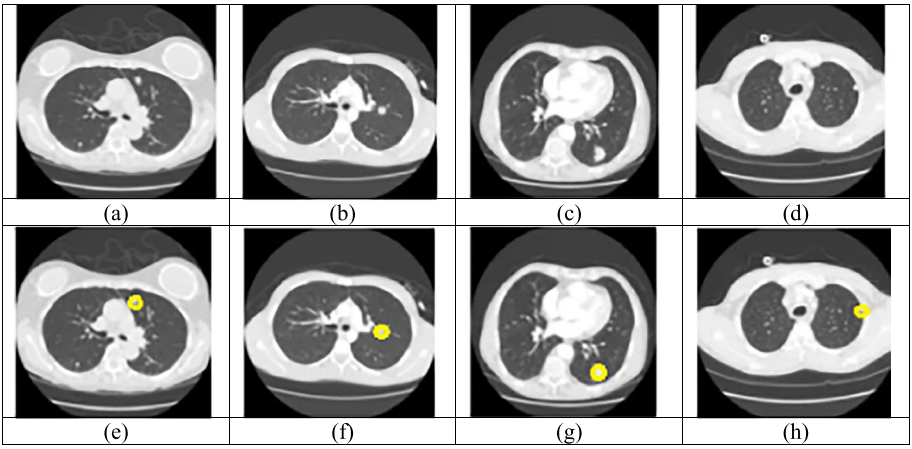

Fig. 4 Sample dataset images, (a-d) Input images and (e–h) segmented images

reconstruction interval, 64 × 0:625 mm collimation, 1.0 helical pitch, 220 mA current, and 120 kV voltage of standard clinical protocol. The scan ranges from 0.58 to 0.98 mm associated with the pixel size via imaging matrix pixels of 512 × 512. In thoracic malignancies of CT imaging, more than ten years of experience and two radiologists annotates all scans. By using Itk snap software, primary tumors on transversal plane boundaries are outlined [30]. Figure 4 explains the sample dataset image.

4.2 Performance metrics

The measures like precision, sensitivity and dice similarity score (DSS), generalized loss and dice loss are quantitatively validating the accuracy of lung tumor segmentation. The ground truth and segmentation results similarities are analyzed through DSS [3, 22, 28].

$$DSS = \frac{2\ true\ positive}{false\ positive\ +2\ \ true\ positive\ +\ false\ negative} \tag{11}$$

$$Sensitivity = \frac{true\ positive}{true\ positive\ +\ false\ negative} \tag{12}$$

$$\mathrm{Pr}ecision = \frac{true\ positive}{true\ positive\ +\ false\ positive} \tag{13}$$

Voxel-wise overlap of each metric between the ground truth and segmentation results are analyzed via precision, recall, and DSS. Better the performance of segmentation with higher values.

The EDCNN model is optimized via the M^2PSO algorithm by utilizing generalized dice loss (GDL) to minimize the data imbalance impact in the case of training.

$$Generalized\ dice\ loss\ = 1 - \frac{2}{K} \sum_{W_k} \frac{W_k \cdot \sum_m P_{mk} Q_{mk}}{(\sum_m P_{mk} + \sum_m Q_{mk})} \tag{14}$$

where M and k are the voxels and classes. The ground truth segmentation maps of one hot encoding are Q and the network softmax output is P. For various label set properties, the weight to provide invariance is $W_k = \frac{1}{(\sum_{m=1}^{M} R_{km})^2}$

An Eq. (15) explains the dice loss;

$$Dice\ loss = 1 - \frac{2}{K} \sum_{W_k} \frac{\sum_m P_{mk} Q_{mk}}{(\sum_m P_{mk} + \sum_m Q_{mk})} \tag{15}$$

The invariance to the various label set properties is provided with generalized dice loss introducing weight W_k compared to dice loss.

4.3 Performance analysis

The performance evaluation of both training and validation accuracy is plotted in Fig. 5. Randomly divide the dataset into two subsets namely 70% for training and 30% for validation. The number of epochs varies from 0 to 50 with respect to varying percentages of accuracy. The X-axis represents a varying number of epochs and the Y-axis signifies the varying number of accuracy. The number of epochs increases by increasing both training and validation accuracy respectively.

The training progress along with the DSS means on the validation set is represented in Fig. 6. The generalized Dice loss function trains all of these networks to 50 epochs. The lowest dice score similarity is obtained by using the deep learning (DL) technique. The other existing methods like DAL and R3-D are higher than the DL model. But, the proposed

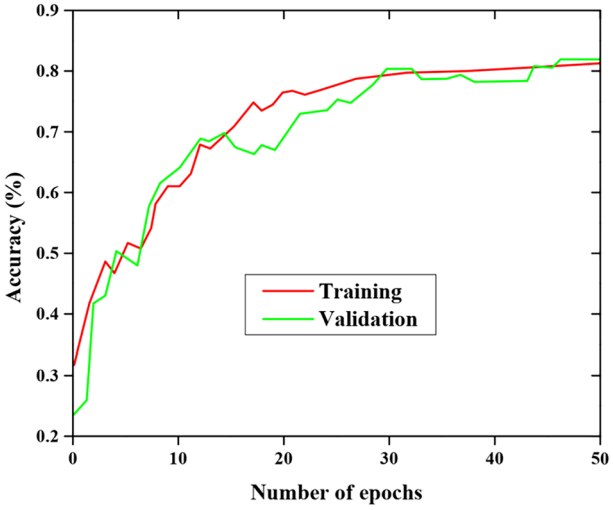

Fig. 5 Training and validation accuracy evaluation

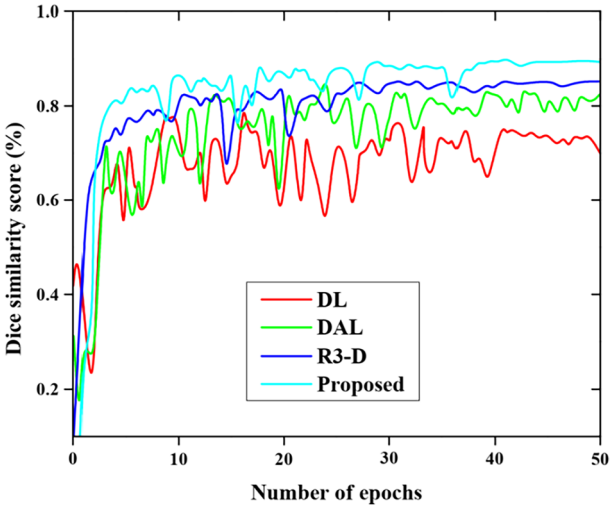

Fig. 6 Training progress along with the DSS mean on the validation set

method has superior performance among all these other techniques such as DAL, DL, and R3-D methods respectively. The DSS of the proposed model is superior to other models and it yielded inferior performances. Table 3 expresses the result of the confusion matrix.

The various loss functions in the learning process are plotted in Fig. 7. The dice loss function with the proposed EDCNN-M^{2}PSO algorithm is examined. The number of epochs varies from 50 with respect to varying percentages of dice loss. The dice loss is superior to the generalized loss function. The pictorial representation of various loss functions with the mean DSS on the set of validation is plotted in Fig. 8. At the 10th epoch, the dice loss with respect to DSS decreases with increasing generalized loss is obtained.

Figure 9 depicts the pictorial representation of segmentation efficiency analysis. The methods such as DL [16], DAL [20], R3-D [14], HSN [9], and proposed EDCNN-M^{2}PSO algorithms are applied to this investigation thereby obtaining varying segmentation output results. The affected regions are successfully extracted and segmented and their performance is shown by using three measures DSS, precision, and sensitivity results with different measures. From this investigation, the proposed method provided superior segmentation results than other existing methods like DL, DAL, R3-D, and HSN respectively.

The overall segmentation efficiency based on average precision, sensitivity, and dice score similarity is represented in Fig. 10. The performance measures like dice score similarity, precision, and sensitivity validate the efficiency of lung cancer segmentation using the EDCNN-M^{2}PSO algorithm. The existing method like DL [16], R3-D [14], and HSN [9] are used in this evaluation. From this investigation, the proposed EDCNN-M^{2}PSO algorithm ideally demonstrated superior segmentation performances in the case of average dice score similarity, precision, and sensitivity than other existing techniques.

Table 3 Confusion matrix

	Actual class or Normal	Predicted class or Abnormal
Actual class or Normal	16	84
Predicted class or Abnormal	86	14

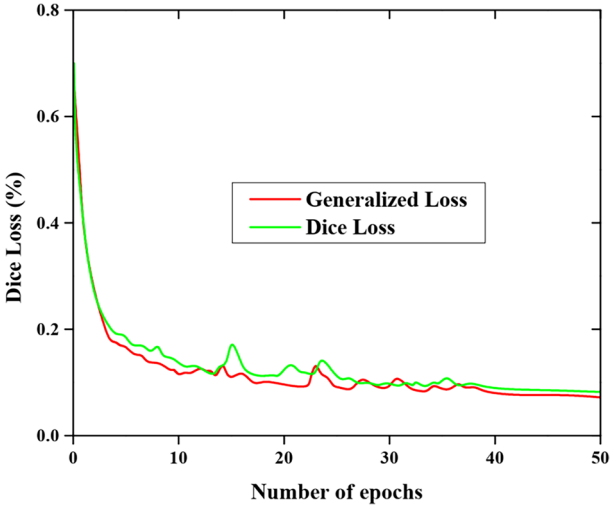

Fig. 7 Various loss functions with the learning process

5 Discussion

The digitization of healthcare services increased the usage of healthcare-related applications. The proposed model can be used for early disease diagnosis if it is implemented in healthcare-related applications. An effective lung disease prediction application can help people diagnose the abnormalities in the lung in the early stage when integrated with a conventional healthcare system. It can also help to monitor the patient's condition and give more information regarding their lung. The performance of the proposed model is evaluated in terms of different performance metrics such as accuracy, sensitivity, precision, DSS, and Dice loss. The M^2PSO algorithm improves the generalization (segmentation capability) and robustness (anti-interference capability) of the EDNN model. It helps to segment the lung tumor from the CT scan by overcoming the issues associated with CT image consistency. The results show that

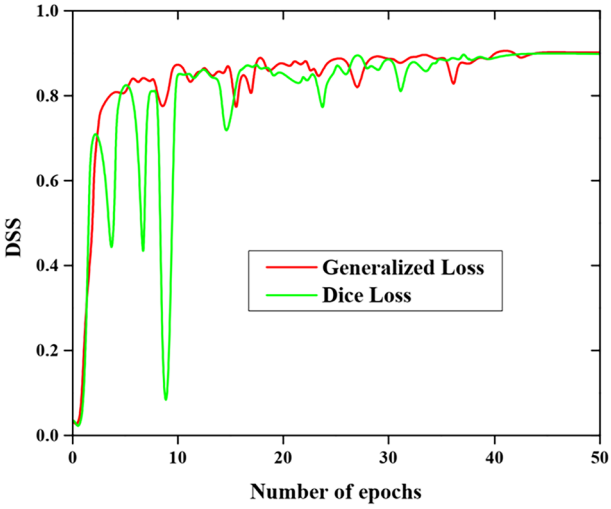

Fig. 8 Various loss functions with the mean DSS on the set of validation

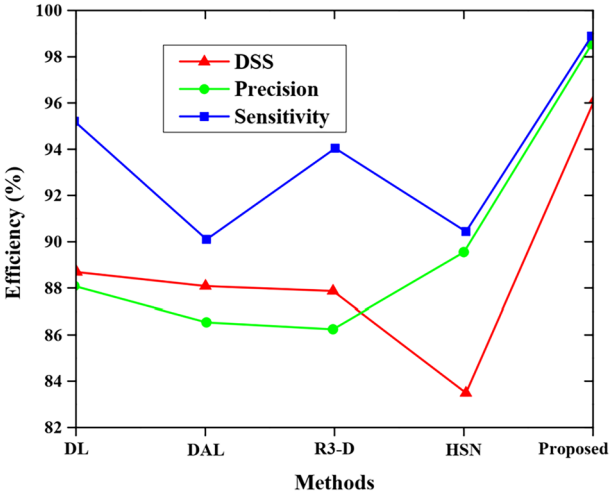

Fig. 9 Segmentation efficiency analysis

the proposed model is effective in terms of different aspects but the different challenges faced by us while conducting this study are specified as follows. Unavailability of labeled datasets, lack of diverse datasets due to hospital unwillingness, and country-specific security legislation prevented us from acquiring high-quality data for training the model. These are the challenges that hindered us from testing our framework fully.

6 Conclusion

This study proposed an ensemble deep convolutional neural network (EDNN) based on Modified mayfly optimization and modified particle swarm optimization (M^2PSO) algorithm to segment the lung tumor images. The proposed model is implemented using MATLAB software. The dataset images were collected from Shandong Cancer Hospital

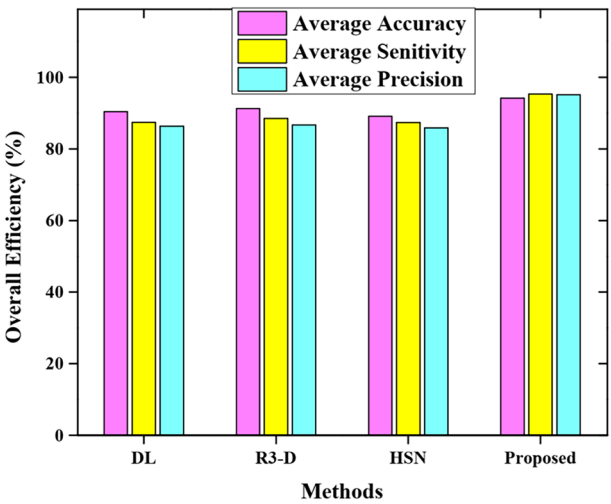

Fig. 10 Overall segmentation efficiency based on average precision, sensitivity, and accuracy

Affiliated with Shandong University (SHFSU). The precision, sensitivity, and dice similarity score (DSS), generalized loss, and dice loss are the performance metrics for analyzing the performance validation of proposed lung tumor segmentation. The proposed technique demonstrated higher training and validation accuracy, as well as the training progress along with the DSS, mean on the validation set. The DSS, precision, and sensitivity results of the proposed method are superior to other existing methods such as DL, DAL, R3-D, and HSN. The proposed model offers an average accuracy, sensitivity, and precision scores of 97%, 98%, and 98%. At the 10^{th} epoch, the dice loss concerning DSS decreases while generalization loss increases. The DSS value of the proposed model is 98.6%, which is relatively higher than the existing techniques such as DL (95.2%), DAL (90%), R3-D(94%), and HSN (90%). In the future, we plan to detect lung cancer by analyzing the small and ground nodules from low-dose CT scans. We also plan to implement this model in a real-time setting in various parts of the world.

Funding Not applicable.

Data availability Data sharing is not applicable to this article as no new data were created or analyzed in this study.

Code availability Not applicable.

Declarations

Conflict of interest The authors declare that they have no conflict of interest.

Human and animal rights This article does not contain any studies with human or animal subjects performed by any of the authors.

Informed consent Informed consent was obtained from all individual participants included in the study.

Consent to participate Not applicable.

Consent for publication Not applicable.

References

1. Abbas A, Abdelsamea MM, Gaber MM (2021) Classification of COVID-19 in chest X-ray images using DeTraC deep convolutional neural network. Appl Intell 51(2):854–864
2. Akter O, Moni MA, Islam MM, Quinn JM, Kamal AHM (2021) Lung cancer detection using enhanced segmentation accuracy. Appl Intell 51(6):3391–3404
3. Albahli S, Nida N, Irtaza A, Yousaf MH, Mahmood MT (2020) Melanoma lesion detection and segmentation using YOLOv4-DarkNet and active contour. IEEE Access 8:198403–198414
4. Anita R, Chaitanyakumar MV (2018) An efficient artificial bee colony algorithm for optimising the design of rectangular microstrip patch antenna. Int J Mobile Network Des Innov 8(1):7–16
5. Aristophanous M, Penney BC, Martel MK, Pelizzari CA (2007) A Gaussian mixture model for definition of lung tumor volumes in positron emission tomography. Med Phys 34(11):4223–4235
6. Baek S, He Y, Allen BG, Buatti JM, Smith BJ, Tong L, Sun Z, Wu J, Diehn M, Loo BW, Plichta KA (2019) Deep segmentation networks predict survival of non-small cell lung cancer. Sci Rep 9(1):1–10
7. Bari M, Ahmed A, Sabir M, Naveed S (2019) Lung cancer detection using digital image processing techniques: A review. Mehran Univ Res J Eng Technol 38(2):351–360
8. Chen K, Franko K, Sang R (2021) Structured model pruning of convolutional networks on tensor processing units
9. Chen W, Wei H, Peng S, Sun J, Qiao X, Liu B (2019) HSN: hybrid segmentation network for small cell lung cancer segmentation. IEEE Access 7:75591–75603

10. Chen X, Duan Q, Wu R, Yang Z (2021) Segmentation of lung computed tomography images based on SegNet in the diagnosis of lung cancer. J Rad Res Appl Sci 14(1):396–403
11. Gordienko Y, Gang P, Hui J, Zeng W, Kochura Y, Alienin O, Rokovyi O, Stirenko S (2018) Deep learning with lung segmentation and bone shadow exclusion techniques for chest X-ray analysis of lung cancer. In International Conference on Computer Science, Engineering and Education Applications (638–647). Springer, Cham
12. Gordienko Y, Gang P, Hui J, Zeng, W, Kochura Y, Alienin O, Rokovyi O, Stirenko S (2018) Deep learning with lung segmentation and bone shadow exclusion techniques for chest X-ray analysis of lung cancer. In International Conference on Computer Science, Engineering and Education Applications (638–647). Springer, Cham
13. Jia H, Xia Y, Song Y, Cai W, Fulham M, Feng DD (2018) Atlas registration and ensemble deep convolutional neural network-based prostate segmentation using magnetic resonance imaging. Neurocomputing 275:1358–1369
14. Kamal U, Rafi AM, Hoque R, Wu J, Hasan MK (2020) Lung cancer tumor region segmentation using recurrent 3d-denseunet. In International Workshop on Thoracic Image Analysis (36–47). Springer, Cham
15. Kavitha P, and Prabakaran S (2019) A novel hybrid segmentation method with particle swarm optimization and fuzzy c-mean based on partitioning the image for detecting lung cancer
16. Li Z, Zhang J, Tan T, Teng X, Sun X, Zhao H, Liu L, Xiao Y, Lee B, Li Y, Zhang Q (2020) Deep learning methods for lung cancer segmentation in whole-slide histopathology images-the acdc@ lunghp challenge 2019. IEEE Journal of Biomedical and Health Informatics
17. Liu X, Li KW, Yang R, Geng LS (2021) Review of Deep Learning Based Automatic Segmentation for Lung Cancer Radiotherapy. Front Oncol 11:2599
18. Manoharan S (2020) Improved version of Graph-cut algorithm for CT images of lung cancer with clinical property condition. J Artif Intell 2(04):201–206
19. Mary NAB, Dharma D (2017) Coral reef image classification employing improved ldp for feature extraction. J Vis Commun Image Represent 49:225–242
20. Men K, Geng H, Biswas T, Liao Z, Xiao Y (2020) Automated quality assurance of OAR contouring for lung cancer based on segmentation with deep active learning. Front Oncol 10:986
21. Mukilan K, Rameshbabu C, Velumani P (2021) A modified particle swarm optimization for risk assessment and claim management in engineering procurement construction projects. Mater Today: Proc 42:786–794
22. Müller D, Rey IS, Kramer F (2020). Automated chest ct image segmentation of covid-19 lung infection based on 3d u-net
23. Onyema EM, Elhaj MAE, Bashir SG, Abdullahi I, Hauwa AA, Hayatu AA, Edeh MO, Abdullahi I (2020) Evaluation of the performance of K-nearest neighbor algorithm in determining student learning styles. Int J Innov Sci Eng Techn 7(1):91–102
24. Onyema EM, Shukla PK, Dalal S, Mathur MN, Zakariah M, Tiwari B (2021) Enhancement of patient facial recognition through deep learning algorithm: ConvNet. J Healthcare Eng
25. Shaheen MA, Hasanien HM, El Moursi MS, El-Fergany AA (2021) Precise modeling of PEM fuel cell using improved chaotic MayFly optimization algorithm. Int J Energy Res 45(13):18754–18769
26. Skourt BA, El Hassani A, Majda A (2018) Lung CT image segmentation using deep neural networks. Procedia Computer Science 127:109–113
27. Sun S, Bauer C, Beichel R (2011) Automated 3-D segmentation of lungs with lung cancer in CT data using a novel robust active shape model approach. IEEE Trans Med Imaging 31(2):449–460
28. Xu M, Qi S, Yue Y, Teng Y, Xu L, Yao Y, Qian W (2019) Segmentation of lung parenchyma in CT images using CNN trained with the clustering algorithm generated dataset. Biomed Eng Online 18(1):1–21
29. Yadav SS, Jadhav SM (2019) Deep convolutional neural network based medical image classification for disease diagnosis. J Big Data 6(1):1–18
30. Yushkevich PA, Piven J, Hazlett HC, Smith RG, Ho S, Gee JC, Gerig G (2006) User-guided 3D active contour segmentation of anatomical structures Significantly improved efficiency and reliability. NeuroImage 31(3):1116–1128
31. Zhang B, Allebach JP (2008) Adaptive bilateral filter for sharpness enhancement and noise removal. IEEE Trans Image Process 17(5):664–678